Hindawi Publishing Corporation
International Journal of Microwave Science and Technology
Volume 2015, Article ID 453710, 9 pages
http://dx.doi.org/10.1155/2015/453710

Research Article

Turn Ratio, Substrates' Permittivity Characterization, and Analysis of Split Ring Resonator Based Antenna

Seyi S. Olokede,[1] Nurul A. Mohd-Razif,[2] and Nor M. Mahyuddin[2]

[1]*Department of Electrical & Electronic Engineering, Olabisi Onabanjo University, PMB 5026, Ifo, Ogun State, Nigeria*
[2]*School of Electrical & Electronic Engineering, Universiti Sains Malaysia, 14300 Nibong Tebal, Penang, Malaysia*

Correspondence should be addressed to Seyi S. Olokede; solokede@gmail.com

Received 30 June 2015; Accepted 8 October 2015

Academic Editor: Walter De Raedt

The turn ratio, coupling space between sections, and substrate permittivity effects on spilt ring resonator (SRR) are investigated. The analysis of the presented SRR with respect to the effects of substrate and number of gaps per ring to further characterize its peculiarities is experimented with miniaturized capability as our intent. Six different SRRs were designed with different turn ratios, and the sixth is rectangular microstrip patch centre-inserted. Different numbers and gap sizes are cut on the SRRs while the gap spacing between the conductors of the SRR was varied to determine their effects taking cognizance of the effects of different substrates. The designs were investigated numerically using 3D finite integration technique commercial EM solver, and the resulting designs were prototyped and subsequently measured. Findings indicate that the reflection coefficient of the MSRR with centre-inserted patch antenna is better compared to MSRR without the patch antenna irrespective of the laminate substrate board, and so is its gain.

1. Introduction

The explosive growth in the demand for wireless communication and information transfer using mobile phone, satellites, and personal communications devices has created the need for advanced antenna design technology. Microstrip planar antennas are smart solutions for compact and cost effective wireless communication systems, in particular due to its significant attractive features of low profile, light weight, easy fabrication, low volume, low profile, ease of integration with printed circuit boards, low power handling capability of printed circuits, and conformability to mounting hosts [1]. Thus, these types of antennas are flexible due to their conformability. As such, smaller antennas are feasible based on the electrodynamics of the patch antenna, though they are limited by their electrical length, in particular the conventional patch antenna.

SRR and its derivatives have been one of the burning issues on antenna miniaturization at microwave and millimeter wave systems in recent times. One very notable attribute that makes SRRs stands out is the increasing need for the optimum usage of space in modern microwave circuits. High Q, low cost, and low radiation loss are extra additives that makes them common technology for filter designs [2–6], antenna design [7–11], and recently applicable in metamaterials [12, 13].

Theoretically, SRR structure exhibits the most common negative permeability characteristics. When the alternating magnetic field is applied perpendicular to the SRR plane, the electromagnetic feature of the SRR can be excited by a time-varying magnetic field with a nonnegligible component applied parallel to the ring axis. This will form a resonant circular current in the ring or rings and hence dictate the resonant frequency. It therefore behaves like a magnetic field driven by inductor and capacitor (LC) resonant tanks that are externally driven by the magnetic field [14].

Hence in a rectangular multiple SRR (MSRR), the conductor trace with opposite sides of the SRR may be treated as coupled line sections. The total inductance is the sum of self-inductance of the sections and the mutual inductance between the turns on assumption that the magnitude and phase of the current across the sections are constant.

On the other hand, SRR has maximum electric field density near the slit and, interestingly, the nature and the intensity of the fringing fields between the gaps, and also the number of rings determines the nature and the strength of the coupling. Ironically, the SRR has the maximum electric charge densities at the gap edges with opposite signs, whereas the current flow is optimum along the ring ribs opposite to the rib.

Therefore the effect of the magnetic field excitation at the perpendicular plane of the SRR with respect to its electromagnetic feature vis-à-vis, its resonance frequency, and the spacing between the parallel coupled sections and the effect of electric field intensity near the slits are examined in this work. Much more, the nature and the extent of the fringing field with respect to different dielectric substrate are investigated.

2. Materials and Methods

The proposed SRR structure consists of N number of concentric split ring resonators to obtain magnetic resonances at distinct frequencies. The value of each frequency can be adjusted by changing the design parameters such as the metal width (w) and gap size (g) for each ring as well as ring to interrings spacing (d). As a result, increasing the number of rings (N) will increase the resonance frequency. Self-inductance also increases when the side length of the metal ring increases with a corresponding decrease in the LC resonance frequency of the resonator, as corroborated by Turkmen et al. [15].

The frequency response of the SRR is obtained using (1), where L_T represent the total equivalent inductance while C_{eq} represent the equivalent capacitance. The L_T value is obtained by using (2a), whereas C_{eq} is obtained using (2b) [16]:

$$f_0 = \frac{1}{2\pi\left(L_T C_{\text{eq}}\right)^{0.5}}, \tag{1}$$

$$L_T = 2\times 10^{-4}\ell\left(2.303\log_{10}\frac{4\ell}{c} - \gamma\right), \tag{2a}$$

$$C_{\text{eq}} = \frac{1}{2}\left(C_0 + C_g\right), \tag{2b}$$

where $\ell = 8a_{\text{ext}} - g$, $C_0 = (4a_{\text{avg}} - g)C_{\text{pul}}$, and, $a_{\text{avg}} = a_{\text{ext}} - w - d/2$. C_0 is the series capacitance between two adjacent rings, C_{pul} is the capacitance per unit length of the ring, γ constant (= 2.853) for wire loop of square geometry, and g is the slit gap, whereas d is the gap between the rings. The equation to calculate C_{pul} is stated in (3) while (4) defines the gap capacitance (C_g) between the slits, whereas ε_r is the relative dielectric permittivity of the substrate, Z_0 is the characteristic impedance (set at 50 Ω), and c is the speed of light

$$C_{\text{pul}} = \frac{(\varepsilon_r)}{cZ_0}, \tag{3}$$

$$C_g = \frac{\varepsilon_0 w}{g}. \tag{4}$$

The dimensions of the SRR were determined using the above equations with g = 3 mm, d = 0.3 mm, and w = 0.5 mm.

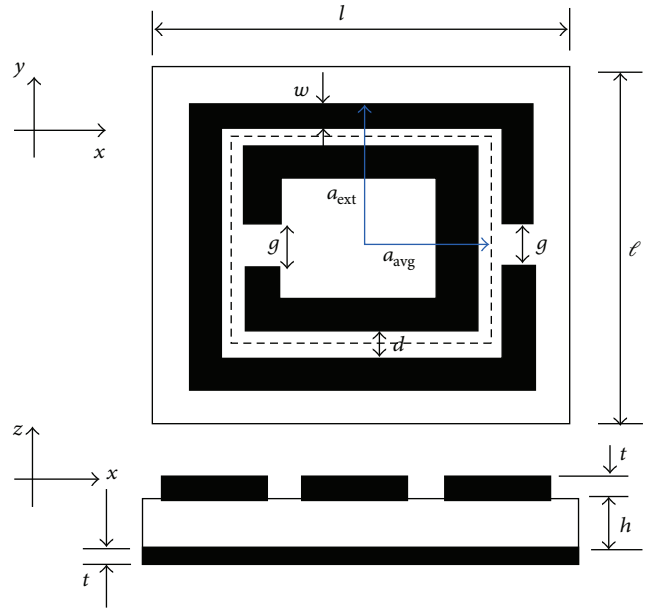

Figure 1: Topology of the proposed SRR.

Figure 1 depicts the geometry of the SRR, Figure 2 is the proposed designs simulated using 3M EM microwave solver, and Figure 3 is the fabricated designs of the propose design. The optimized prototypes of the proposed were photoetched on (1) Roger duroid laminate microwave substrate of permittivity (ε_r) of 3.38, height of 0.813 mm, and metallization of 35 μm; (2) duroid permittivity (ε_r) of 6.45, height of 2.5 mm, and metallization of 35 μm; (3) FR4 epoxy substrate of permittivity (ε_r) of 2.4, height of 1.6 mm, and metallization of 35 μm; and, finally, (4) FR4 of permittivity (ε_r) of 4.4, height of 5 mm, and metallization of 35 μm. The resulting designs were tested using the HP 8720D (50 MHz–20 GHz) network analyzer in order to measure the reflection coefficients, the antenna impedance, and the voltage standing wave ratio (VSWR). For this measurement process, HP 8720D (50 MHz–20 GHz) network analyzer was used to measure the reflection coefficient, resonant frequency, bandwidth, and input impedance. For bandwidth measurement, −10 dB point was used to determine the range of frequency. Prior to measurement, a kit is required to calibrate the network analyzer at the frequency required for one port only. The recorded data from the network analyzer measurement was plotted and compared with simulated results. The connection configuration of the network analyzer is shown in Figure 4(a).

The radiation pattern characteristics of these fabricated antennas represent graphically their radiation properties as a function of space coordinates. These properties are the power density, radiation intensity, field strength, directive phase, and polarization.

The measurement of the radiation patterns was done using HP 83620B (10 MHz to 20 GHz) signal generator, transmitting antenna, a rotating machine, and Agilent 8565E (9 KHz–50 GHz) spectrum analyzer, whereas each antenna under measurement (AUT) was attached to the rotating machine where the AUT acts as a receiving antenna.

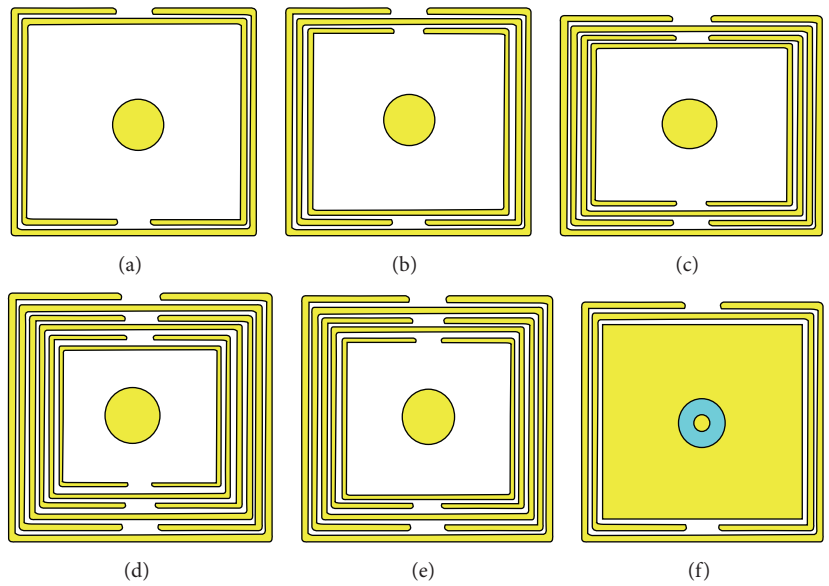

Figure 2: The proposed SRR designs (a) $N = 2$, (b) $N = 3$, (c) $N = 4$, (d) $N = 5$, (e) $N = 6$, and (f) $N = 2$ patch inserted.

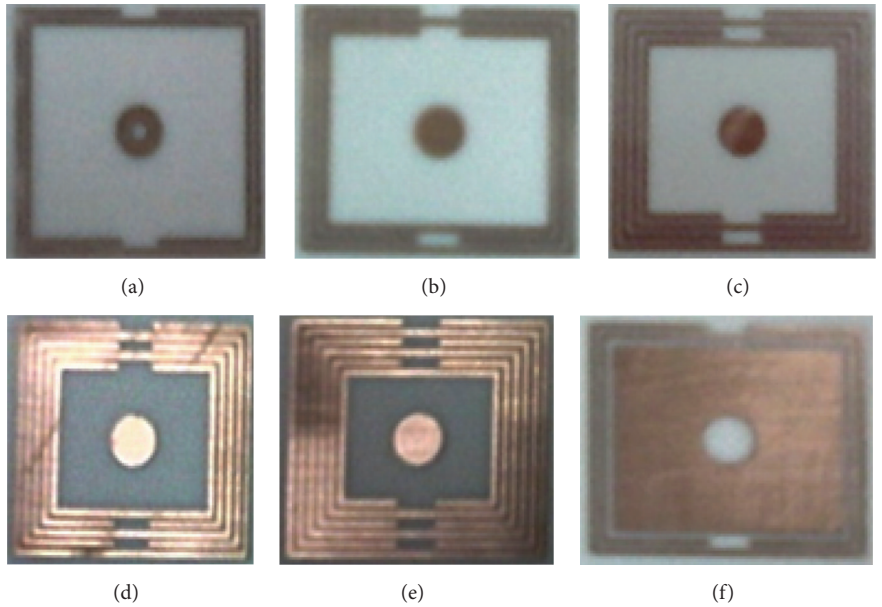

Figure 3: The fabricated SRR designs (a) $N = 2$, (b) $N = 3$, (c) $N = 4$, (d) $N = 5$, (e) $N = 6$, and (f) $N = 2$ centre patch inserted.

The transmitting antenna used is a standard dipole antenna. Both receiving and transmitting antenna were placed such that both of them were aligned with each other. The normalized input power data of each 10° was subsequently used to plot radiation pattern on the polar graph for each of the designed antennas. The measured radiation patterns were finally compared with the radiation patterns from the 3D EM simulated results. The measurements were done two times for each antenna design. First, the copolarization in the E plane was measured. Both the receiving and transmitting antennas were placed in vertical positions where the receiving antenna was rotated 360° while the measured data was recorded. The next step was to measure the copolarization in the H-copolarization. Both receiving and transmitting antennas were placed in horizontal positions. Then the receiving antenna was rotated 360° while the measured data was recorded. Then, normalized input power data for each 10° was used to plot radiation pattern on the polar graph for each of designed antennas. The testing arrangement for gain measurement is the same as in Figure 4(b). According to IEEE Standard Test Procedures for Antennas, ANSI/IEEE Std 149-1979, the most commonly employed method for antenna gain measurement is gain-transfer (gain-comparison) method. This technique utilizes a gain standard antenna to determine

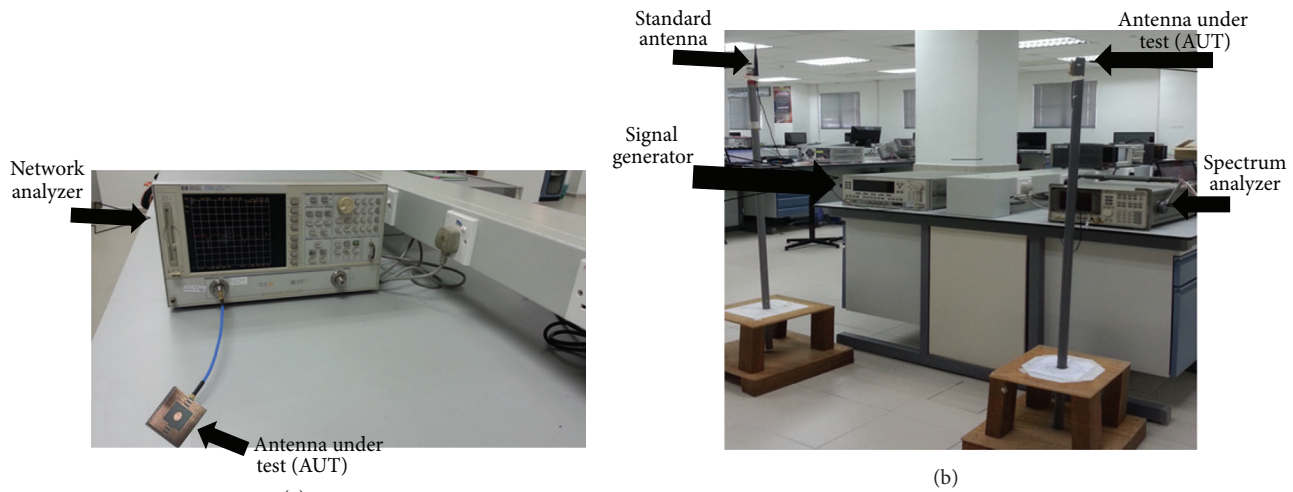

Figure 4: Equipment setup measurement. (a) Reflection coeff. (b) Radiation pattern and impedance matching.

the absolute gains. The procedure requires two sets of measurements. In one set, using the test antenna as receiving antenna, the received power (P_T) was recorded. In the other set, the test antenna was replaced by the standard gain antenna and the received power (P_S) was recorded. In both sets, the geometrical arrangement was maintained intact, and the input power was maintained the same. This method is deployable both in the anechoic chamber and in open space. Equation (5) was used to calculate the gain of the AUT as follows:

$$(G_T)_{\mathrm{dB}} = (G_S)_{\mathrm{dB}} + 10\log_{10}\left(\frac{P_T}{P_S}\right), \tag{5}$$

where G_T is the gain of tested antenna, G_S is the gain of standard antenna, P_T is the power received by tested antenna, and P_S is the power received by the standard antenna. Equation (5) can be written as

$$G_T\,(\mathrm{dB}) = P_T\,(\mathrm{dBm}) - P_S\,(\mathrm{dBm}) + G_S\,(\mathrm{dB})\,. \tag{6}$$

If the test antenna is circularly or elliptically polarized, gain measurements using the gain-transfer method can be accomplished by at least two different methods. One way would be to design a standard gain antenna that possesses circular or elliptical polarization. This approach would be attractive in mass productions of power-gain measurements of circularly or elliptically polarized antennas (ANSI/IEEE Std 149-1979, 1979). The other way would be to use a standard linearly polarized antenna. Thus, the gain of the AUT has to be measured in two orthogonal orientations. In these types of measurements, the first method would require a standard known gain helical antenna. However, this is outside the scope of our work seeing that the propose designs are linearly polarized. The effects of number of turns (N), gap size (g), and inter-ring spacing (d) and, finally, effect of different substrates permittivity (ε_r) were examined both experimentally and through numerical method. These effects were first parametrically investigated using 3D EM commercial solver and, secondly, were investigated analytically. The findings are presented in Section 3.

3. The Results and Discussions

Figure 5 depicts the simulated and measured reflection coefficient of the multiple SRR (MSRR) with respect to different substrates. Figure 5(a) is the simulated frequency pattern, whereas measured frequency response is shown in Figure 5(b). Table 1 summarizes the performance profile of the proposed based on Roger duroid 4003C substrate. Figures 5 and 6 are similarly based on the same substrate. The resonance occurred at an average frequency of 12.4 GHz as against 12 GHz target frequency with an average differential of 3.33% notwithstanding the value of the turn ratio (N). The reflection coefficients are also reasonable and agreed to a large extent.

The input impedances are largely resistive and marginally reactive. Therefore, instead of storing energy, the electromagnetic energy is properly radiated as supported by the reasonable gain exhibited by the designs across the numbers of turn ratios (N). The standing wave ratios (VSWR) are also commensurate and appropriate. It is observed that resonance occurred at 12 GHz for $N = 2$ in both simulated and measured patterns.

In particular, it is observed that, as $N > 2$, the frequency responses shift to the right hand, indicating higher frequency though with a marginal value of 0.3 GHz. By antenna theory, the only feasible reason for this is if a smaller size dimension is obtained. On the contrary, the aperture size becomes larger as N increases. In Figure 5(b), the shift was left hand side by an amount equal to 0.5 GHz. Seeing that these observations contradict themselves when comparing both simulated and measured frequency patterns, it is definitely certain that there is another factor that could be responsible other than aperture effect. It was observed that as inter-ring spacing d decreases, the coupling becomes stronger and the reflection coefficient improves significantly. In effect, this also shifts the frequency. In addition, the fringing fields' effect is experienced at the gap ends of the gap edges, which inadvertently increases the effective length of the SRR conductor trace, thus shifting the frequency as a result. Much more, the conductor trace forms

Table 1: The performance results of the propose.

Parameters	Output results					
	$N = 2$	$N = 3$	$N = 4$	$N = 5$	$N = 6$	Average
Centre freq., GHz	12.38	12.34	12.39	12.43	12.44	12.396
Reflection coeff., S_{11} (dB)	−23.53	−24.16	−25.1	−24.59	−25.68	−24.612
Input impedance, Ω	46.68 + j0.4	49.4 + j0.1	44.94 + j0.6	50.23 + j0.4	50.67 + j0.3	48.384 + j0.36
Gain (dBi)	6.55	6.58	6.59	6.59	6.93	6.698
VSWR	1.14 : 1	1.13 : 1	1.12 : 1	1.12 : 1	1.11 : 1	1.124 : 1

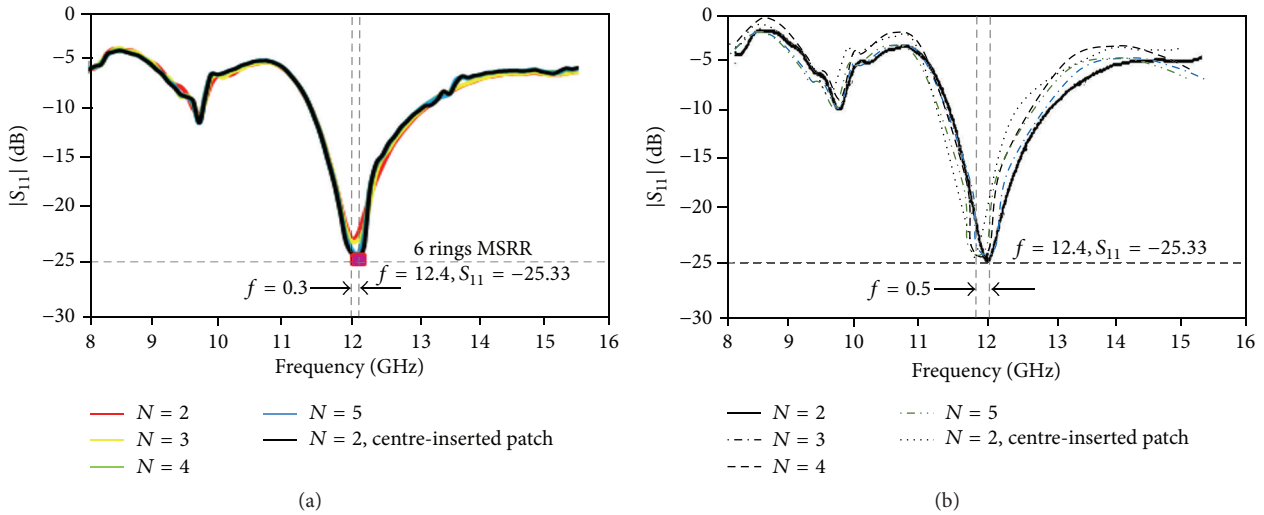

Figure 5: The proposed SRR designs: (a) simulated and (b) measured.

lumped inductance with magnetic field effect and as such the inductive contribution. The gaps between the rings also form the capacitive effects and thus their respective capacitive contributions. This value increases as the turn ratio increases. In effect, these properties affect the performance of these designs significantly.

In Figure 6, the simulated and measured radiation patterns across the impedance bandwidth of 11.5–12.4 GHz are presented in both xz- and yz-planes. In all, the sole maxima occurred at the boresight, and the radiated energy in all is generally directional, though marginal values of back lobes in few of the patterns were noticed. It is noted that the gain of the antennas increases with increases in the number of rings (N). There are not any established findings where variance of gap size (g) and inter-ring spacing (d) influences the gain in any way. Ironically, the effects of gap size (g) on resonance frequency with respect to different substrate are demonstrated in Figure 7, whereas the effects of inter-ring spacing (d) on resonance frequency with respect to different substrate are depicted in Figure 8.

In both figures, the numerical results using 3D EM computer simulation, theoretical results, and experimental results using the stated equations are plotted in order to compare the level of agreement. In Figure 7, resonance responses vary marginally with varying gap sizes and are most noticeable for substrate with substrate dielectric constant of 3.38 notwithstanding the resonant frequency of consideration. Similar observation was noticed in Figure 8 but much significant for substrate with substrate dielectric constant of 6.42 as inter-ring spacing increases. Similar observation was noticed for substrate with substrate dielectric constant of 2.40.

Table 2: The performance results of the propose.

Number of gaps/rings	Varied gap size (mm)	Turn ratio N	Simulated S_{11}
1	0.25	2	−23.58
1	0.50	3	−24.16
1	0.75	4	−24.59
1	1.00	5	−25.68
1	1.25	6	−24.61

Table 2 also summarizes the effects of the number of gap sizes on the reflection coefficients. Finding indicates that neither the numbers of turn ratios (N) nor the number of gap sizes (g) per turn influences the reflection coefficients significantly.

4. Conclusions

The effects of turn ratio (N), gap size (g), inter-ring spacing (d), and, finally, the dielectric constant of the substrate (ε_r) were examined both analytically and numerically. These values were varied and the resulting designs were fabricated on four types of substrates, namely, Roger duroid 4003C, 6010,

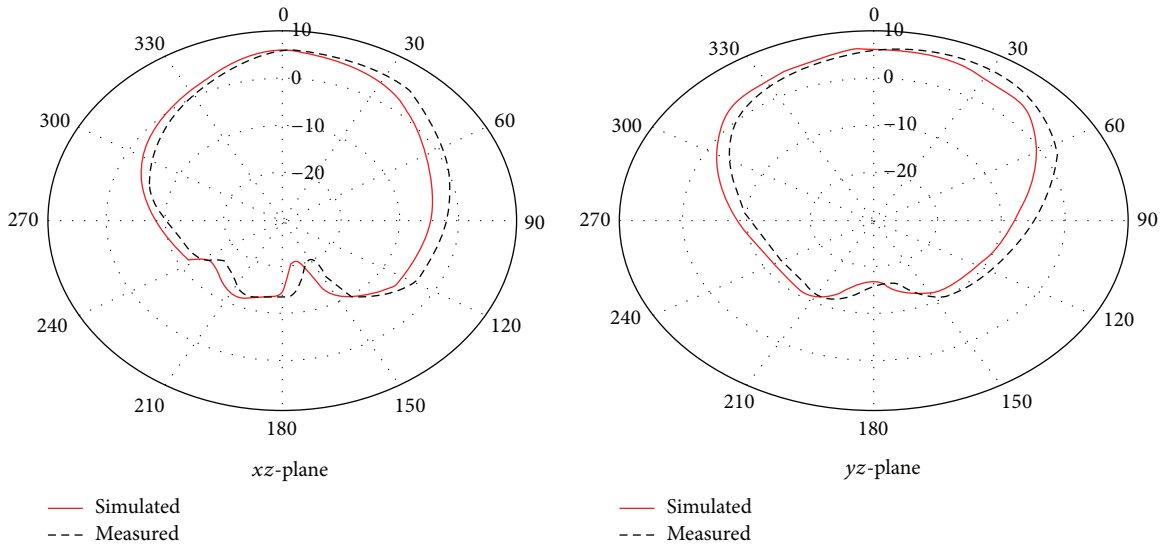

(a)

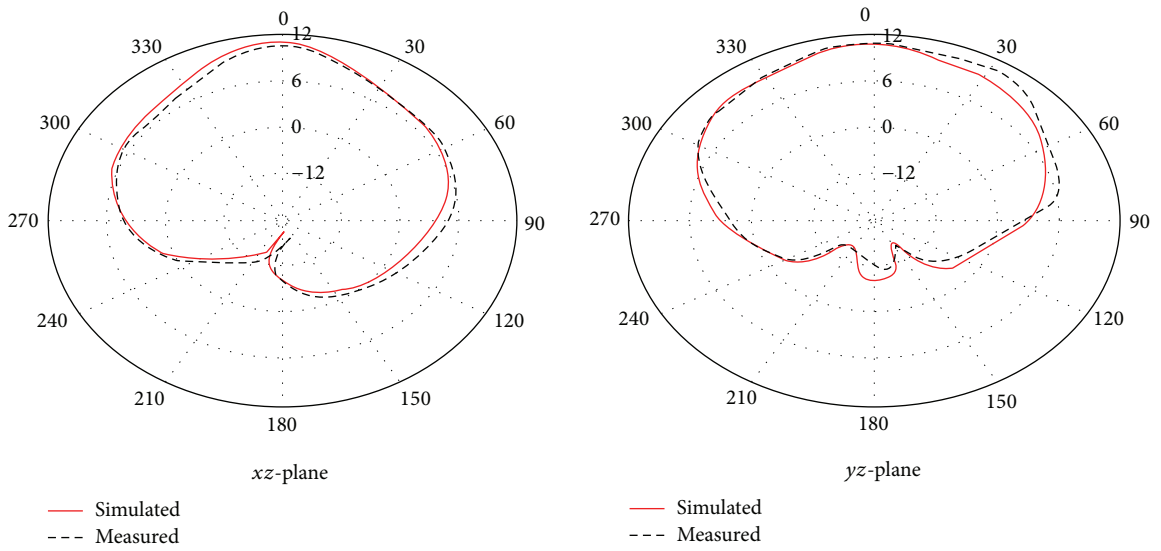

(b)

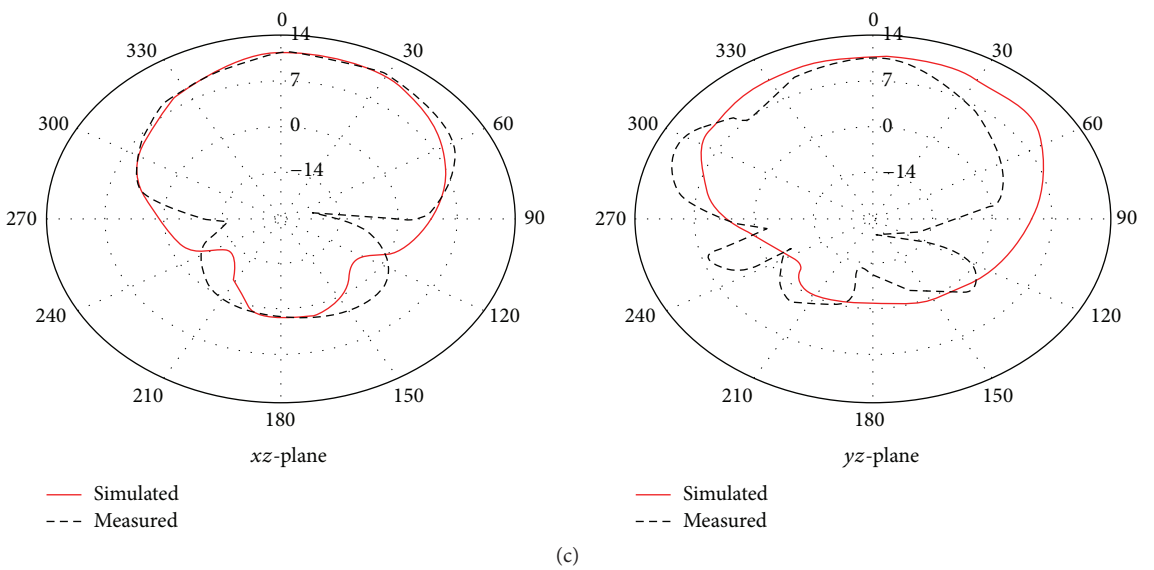

(c)

Figure 6: Continued.

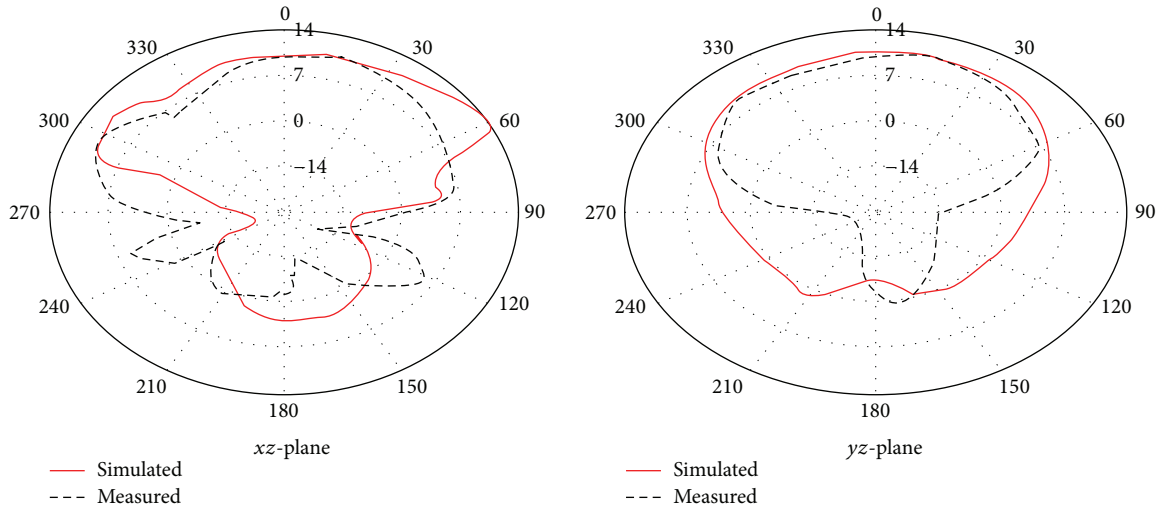

(d)

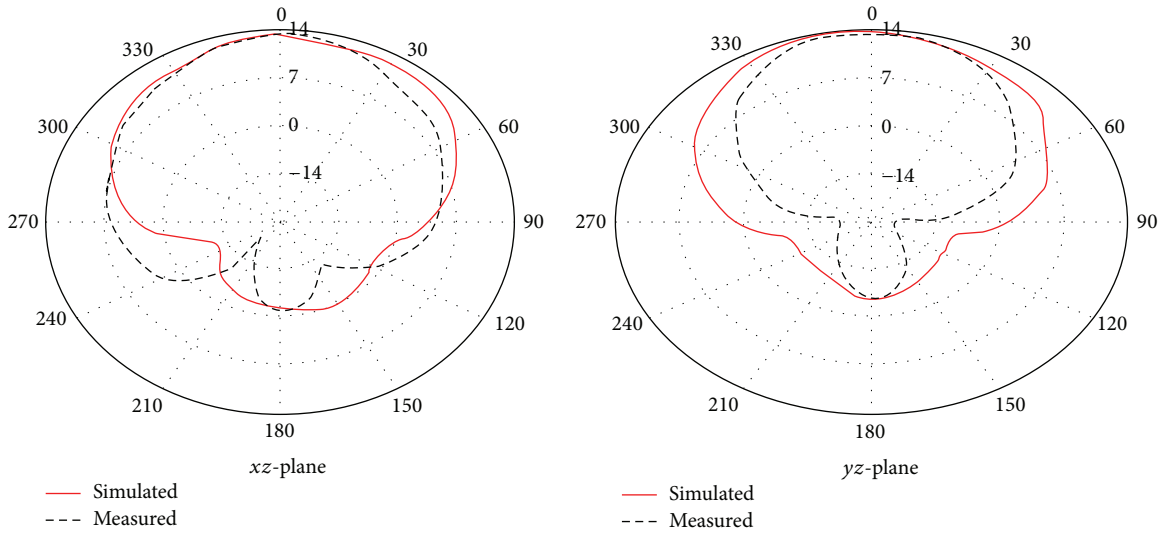

(e)

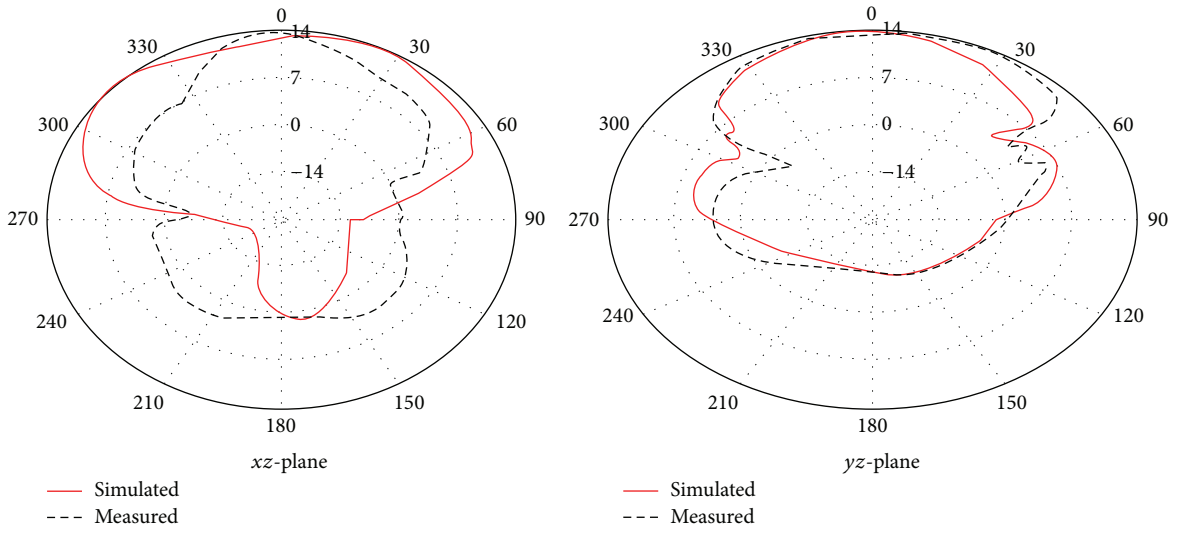

(f)

FIGURE 6: The simulated and measured radiation pattern of the proposed SRR. (a) $N = 2$, (b) $N = 3$, (c) $N = 4$, (d) $N = 5$, (e) $N = 6$, and (f) $N = 2$ patch inserted.

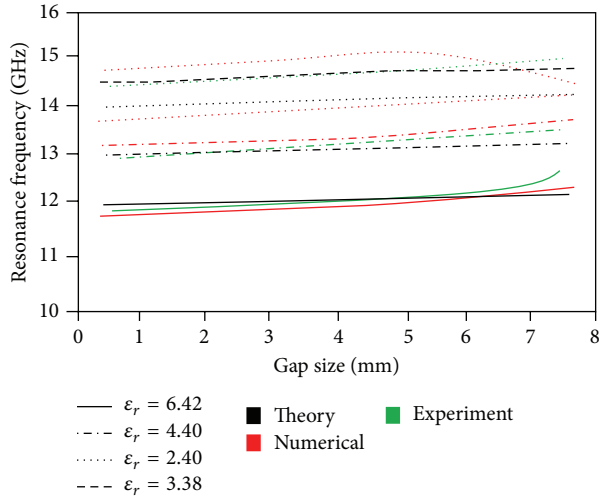

FIGURE 7: The effect of gap size (g) on the resonance frequency.

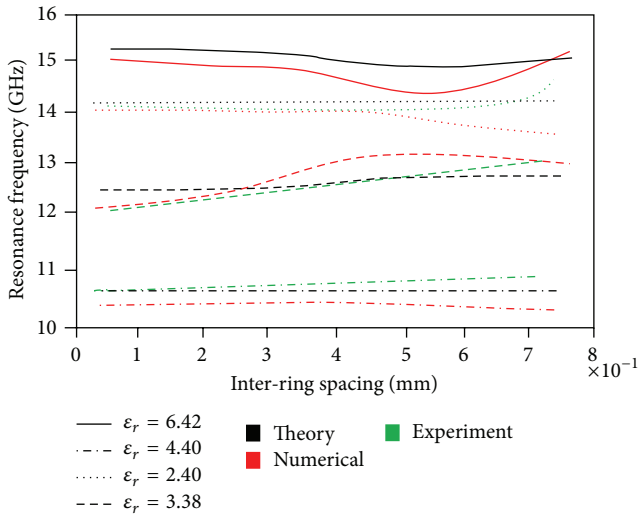

FIGURE 8: The effect of interring spacing (d) on the resonance frequency.

and Epoxy FR4 with dielectric constants of 2.4 and 6.42. Their respective effects on the designed antennas were investigated using numerical solution (via computer simulation) and theoretical formulas. Findings indicate that (1) the reflection coefficients are affected by neither the number of turn ratios, the gap size, nor the number of gap sizes per turn; (2) the gain improves as the turn ratio increases, whereas the gain of the centre-inserted patch proves to be better; and (3) the resonance frequency shifts away from the frequency of consideration as the gap sizes vary.

Conflict of Interests

The authors declare that there is no conflict of interests regarding the publication of this paper.

References

[1] Z. Yu and W. Qi, "A multi-band small antenna based on deformed split ring resonators of left-handed meta-materials," in *Proceedings of the IEEE International Symposium on Microwave, Antenna, Propagation and EMC Technologies for Wireless Communications (MAPE '07)*, pp. 531–534, IEEE, Hangzhou, China, August 2007.

[2] F. Falcone, T. Lopetegi, J. D. Baena, R. Marqués, F. Martín, and M. Sorolla, "Effective negative-ε stop-band microstrip lines based on complementary split ring resonators," *IEEE Microwave and Wireless Components Letters*, vol. 14, no. 6, pp. 280–282, 2004.

[3] A. Vélez, F. Aznar, J. Bonache, M. C. Velázquez-Ahumada, J. Martel, and F. Martín, "Open Complementary Split Ring Resonators (OCSRRs) and their application to wideband cpw band pass filters," *IEEE Microwave and Wireless Components Letters*, vol. 19, no. 4, pp. 197–199, 2009.

[4] J. Bonache, I. Gil, J. García-García, and F. Martín, "Novel microstrip band pass filters based on complementary split-ring resonators," *IEEE Transactions on Microwave Theory and Techniques*, vol. 54, no. 1, pp. 265–271, 2006.

[5] J. Martel, J. Bonache, R. Marqués, F. Martín, and F. Medina, "Design of wide-band semi-lumped bandpass filters using open split ring resonators," *IEEE Microwave and Wireless Components Letters*, vol. 17, no. 1, pp. 28–30, 2007.

[6] R. H. Geschke, B. Jokanovic, and P. Meyer, "Filter parameter extraction for triple-band composite split-ring resonators and filters," *IEEE Transactions on Microwave Theory and Techniques*, vol. 59, no. 6, pp. 1500–1508, 2011.

[7] H. Zhang, Y.-Q. Li, X. Chen, Y.-Q. Fu, and N.-C. Yuan, "Design of circular polarisation microstrip patch antennas with complementary split ring resonator," *IET Microwaves, Antennas & Propagation*, vol. 3, no. 8, pp. 1186–1190, 2009.

[8] H. Zhang, Y.-Q. Li, X. Chen, Y.-Q. Fu, and N.-C. Yuan, "Design of circular/dual-frequency linear polarization antennas based on the anisotropic complementary split ring resonator," *IEEE Transactions on Antennas and Propagation*, vol. 57, no. 10, pp. 3352–3355, 2009.

[9] Y. Dong, H. Toyao, and T. Itoh, "Design and characterization of miniaturized patch antennas loaded with complementary split-ring resonators," *IEEE Transactions on Antennas and Propagation*, vol. 60, no. 2, pp. 772–785, 2012.

[10] B. D. Braaten and M. A. Aziz, "Using meander open complementary split ring resonator (MOCSRR) particles to design a compact UHF RFID tag antenna," *IEEE Antennas and Wireless Propagation Letters*, vol. 9, pp. 1037–1040, 2010.

[11] B. D. Braaten, "A novel compact UHF RFID tag antenna designed with series connected Open Complementary Split Ring Resonator (OCSRR) particles," *IEEE Transactions on Antennas and Propagation*, vol. 58, no. 11, pp. 3728–3733, 2010.

[12] M. Gil, J. Bonache, J. Selga, J. García-García, and F. Martín, "Broadband resonant-type metamaterial transmission lines," *IEEE Microwave and Wireless Components Letters*, vol. 17, no. 2, pp. 97–99, 2007.

[13] M. Durán-Sindreu, A. Vélez, F. Aznar, G. Sisó, J. Bonache, and F. Martín, "Applications of open split ring resonators and open complementary split ring resonators to the synthesis of artificial transmission lines and microwave passive components," *IEEE Transactions on Microwave Theory and Techniques*, vol. 57, no. 12, pp. 3395–3403, 2009.

[14] F. Karshenas, A. R. Mallahzadeh, and J. Rashed-Mohassel, "Size reduction and harmonic suppression of parallel coupled-line bandpass filters using defected ground structure," in *Proceedings of the 13th International Symposium on Antenna Technology and Applied Electromagnetics and the Canadian Radio Science Meeting (ANTEM/URSI '09)*, pp. 1–6, IEEE, Toronto, Canada, February 2009.

[15] O. Turkmen, E. Ekmekci, and G. T. Sayan, "A new multi-ring SRR type metamaterial design with multiple magnetic resonances," in *Proceedings of the Progress in Electromagnetics Research Symposium (PIERS '11)*, pp. 315–319, Marrakesh, Morocco, March 2011.

[16] C. Saha, J. Y. Siddiqui, and Y. M. M. Antar, "Theoretical investigation of the square split ring resonator," in *Proceedings of the IEEE WIE National Symposium on Emerging Technologies (WieNSET '07)*, Kolkata, India, June 2007.